

A numerical study on behavior of CFRP strengthened shear wall with opening

Kiachehr Behfarnia* and Ahmadreza Shirneshan^a

Department of Civil Engineering, Isfahan University of Technology, Isfahan, 84156-83111, Iran

(Received July 30, 2016, Revised November 26, 2016, Accepted December 1, 2016)

Abstract. Concrete shear walls are one of the major structural lateral resisting systems in buildings. In some cases, due to the change in the occupancy of the structure or functional requirements like architectural and even mechanical ones, openings need to be provided and installed in structural walls after their construction. Providing these openings may significantly influence the structural behavior of the constructed wall. This paper considers the results of a nonlinear finite element analysis of shear walls with opening strengthened by carbon fiber reinforced polymer (CFRP) strips with different configurations. Details of bond-slip constitutive model of link elements to simulate the connections of FRP strips to concrete surface is presented. The proposed model in this research has been validated using experimental results available in the literature. The results indicated that the proposed configuration of CFRP strips significantly improved the lateral resistance and deformation capacity of the shear walls with opening.

Keywords: concrete; shear wall; opening; nonlinear finite element; strengthening; CFRP

1. Introduction

Shear walls are common lateral load carrying systems used in many reinforced concrete buildings for resistance against such lateral forces as earthquakes and winds. Sometimes, it is unavoidable to have openings such as doors, windows, and other types in shear walls. These openings may significantly impress the behavior of wall, in such ways as changing its force transition mechanism, reducing its resistance and stiffness, decreasing its ductility level and causing stresses which cannot be classified in the known patterns (Meftah *et al.* 2007, Sengupta and Li 2014, Shariq *et al.* 2008, Behfarnia and Sayah 2012, Kim and Vecchio 2008). Also, there are cases, like the change in occupancy of a building, in which an opening need to be provided in a constructed shear wall that is not designed for its effects. In these cases, the behavior of the wall and its possible strengthening should be studied. The main focus of this study was on these types of shear walls.

In recent years, the rehabilitation and strengthening of structures using bonded fiber-reinforced polymer (FRP) strips have become a cost-effective option, as compared to other alternatives. Some of these advantages are: low density, high tensile strength/weight ratio, high tensile modulus/weight ratio, high performance against the corrosion and good fatigue characteristics (ACI Committee 440 2008, Rezaiefar 2013, Mostofinejad and Aanei 2012, Li *et al.* 2013).

Research on the behavior of reinforced concrete (RC) members with externally bonded FRP has been mainly concentrated on columns and beams, whereas there are limited experimental and analytical studies investigating the effectiveness of FRP retrofitting and strengthening the RC structural walls with or without openings.

Most studies on the rehabilitation of shear walls by FRP strips are experimental. Lombard *et al.* (1999) performed the strengthening of shear walls using carbon fiber reinforced polymer (CFRP) to increase its strength and ductility. In this study shear walls were strengthened by CFRP strips oriented in the vertical direction to the two faces of the walls. The results showed the improvement of flexural capacity secant stiffness at yield. Altin and Koprman (2013) studied the hysteretic behavior of strengthened shear deficient RC walls by CFRP strips under the lateral loadings experimentally. Shear walls in their study were strengthened using different CFRP strip configurations. The results showed CFRP strips significantly improves the behavior of shear walls under the cyclic lateral loading and the strip configurations have a significant effect on the behavior of the strengthened walls and failure mode. Li and Lim (2010) has done a study about the effect of using CFRP strips on the lateral strength and ductility of the non-seismic RC shear walls. The work compared the behavior of damaged RC shear walls after they had been Retrofitted to that of its original shear walls. From the experiments, it was found that the repair of damaged walls using FRP strips could serve to restore the strength and ductility of damaged RC walls. Cruz-Nogues *et al.* (2014) studied the repair and strengthening of RC shear walls using the externally bonded FRP. In repair and strengthening applications, the FRP system was shown to increase the flexural resistance of damaged and undamaged walls.

*Corresponding author, Associate Professor
E-mail: kia@cc.iut.ac.ir

^aGraduate Student
E-mail: ahmadshirneshan@yahoo.com

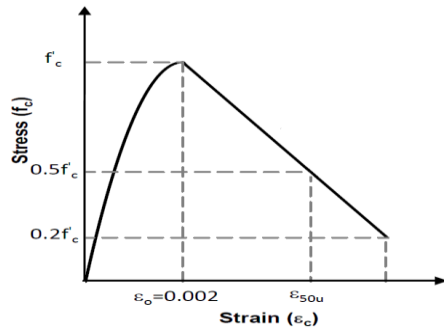


Fig. 1 Modified Kent and Park stress-strain relationship for concrete in compression (adapted from Reddiar 2009)

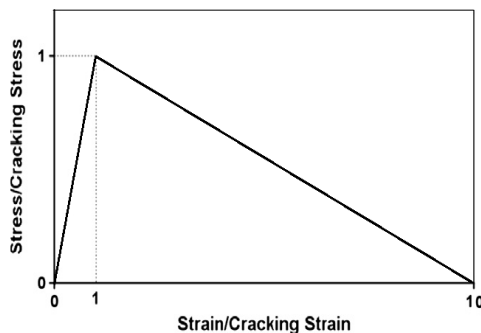


Fig. 2 Stress-strain relationship for concrete in tension (adapted from Mostofinejad and Aanei 2012)

Meftah *et al.* (2007) investigated the seismic analysis of coupled shear walls strengthened by bonded composite plates. This analysis showed the influence of the fibers on the lateral Behavior of coupled shear walls. Li *et al.* (2013) has done experimental and analytical study on Retrofitting Damaged Structural Walls with Openings by Externally Bonded FRP Strips. The strut-and-tie approach was utilized to design the repair schemes. The repaired walls showed the recovery of strength, energy and stiffness of walls.

Typically, the performance of a retrofitted RC shear walls is evaluated experimentally through assessing its hysteretic lateral force-displacement relationships. Although experimental testing seems to be the most evident approach to assess the performance of shear walls with openings, numerical simulations may provide valuable tools for parametric studies and evaluation of the response of RC shear walls.

The current study mainly concentrated on the behavior of RC shear walls with openings strengthened by CFRP composites under monotonic loading using Finite Element (FE) method. This paper also presents details of the proposed bond-slip constitutive model developed for link elements to simulate the connections of FRP strips to concrete (Lu *et al.* 2005).

2. Numerical modeling

Numerical analyses were carried out using a nonlinear finite element commercially available software, ABAQUS/Standard (Version 6.12), appropriate to

structures subjected to static and dynamic loading.

2.1 Modeling of concrete

For the modeling of concrete, the constitutive model used to analyze the concrete was a concrete damaged plasticity model available in ABAQUS. The concrete damaged plasticity model, which is based on the scalar damage, is designed for applications in which concrete is subjected to different conditions of loading, including static and dynamic loading. The model takes into consideration the degradation of the elastic stiffness induced by plastic straining, both in tension and compression (ABAQUS 2012, Li *et al.* 2005, Chen 2007). This model is a continuum plasticity-based damage model for concrete. In this mode, compressive crushing and tensile cracking are the two main failure mechanisms and damaged plasticity is used to model the uniaxial tensile and the compressive response of concrete. Under uniaxial tension, the stress-strain response follows a linear elastic relationship until reaching the failure stress, σ_{10} , which represents the onset of micro-cracking in the concrete material. Beyond this failure stress, the formation of micro-cracks is represented macroscopically with a softening stress-strain response. On the other hand, under uniaxial compression, the response is linear until reaching the value of initial yield, σ_{co} . In the plastic regime, the response is typically characterized by some stress hardening followed by strain softening beyond the ultimate stress, σ_{cu} (ABAQUS 2012, Li *et al.* 2005, Chen 2007).

For modeling the concrete in concrete damage plasticity, the stress-strain curve of concrete in compression and tension is needed. For stress-strain curves of concrete in compression, the modified Kent and Park model, Fig. 1, was chosen where the stress-strain relationship was presented as shown in Eqs. (1) and (2) (Reddiar 2009). For stress-strain curves of concrete in tension, the linear-elastic with the slope of E being up to the tensile strength of concrete was used for stress-strain behavior, also the tension stiffening was used to model the post failure behavior, which allowed for the strain softening behavior of the cracked concrete. In this study, a linear post failure stress-strain relationship defined tension stiffening effect, as shown in Fig. 2, where failure tensile strain was taken to be 10 times of the cracking strain ϵ_{cr} (Mostofinejad and Aanei 2012).

$$f_c = f'_c \left[\frac{2\epsilon_c}{\epsilon_0} - \left(\frac{\epsilon_c}{\epsilon_0} \right)^2 \right] \quad (1)$$

$$\epsilon_{50u} = \frac{3 + 0.29f'_c}{145f'_c - 1000} \quad (f'_c \text{ in MPa}) \quad (2)$$

8-node 3-D solid elements were used to model the concrete. These elements had three degrees of transitional freedom in each node. These elements were able to consider plastic deformation and cracking in three orthogonal directions at each integration point.

2.2 Modeling of steel reinforcement and stirrups

Two dimensional truss elements were used to model the

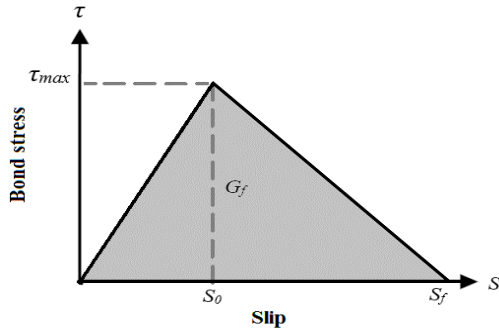


Fig. 3 Bond-slip relationships for FRP-concrete interfaces

steel reinforcement and stirrups and these elements were embedded in concrete solid elements. The steels were considered as elastic-perfectly-plastic materials in both tension and compression. For stress-strain curves of steel, a small positive value was assigned to the slope of the stress-strain curve in the plastic region for avoiding numerical instability. The main parameters of steel materials, such as yield strength, Young's modulus and ultimate strength, were obtained from the experimental study.

2.3 Modeling of FRP strips

The FRP materials were assumed to be orthotropic and the brittle material was supposed to be with zero compressive strength. The mechanical properties were the same in any direction perpendicular to the fibers. Linear elastic properties were assumed for FRP composites and 8-node solid elements were used to model FRP strips (Mostofinejad and Anaei 2012).

2.4 Modeling of FRP de-bonding

In most RC elements repaired/strengthened with FRP, de-bonding of the FRP material from the concrete substrate controls the failure mode and the overall response of the element. Some important de-bonding failure modes are cover separation, plate end interfacial de-bonding, intermediate (flexural or flexural-shear) crack (IC) induced interfacial de-bonding, and critical diagonal crack (CDC) induced interfacial de-bonding. The behavior of the interface between the FRP and the concrete is the key factor controlling de-bonding failures in FRP-strengthened RC structures (Lu *et al.* 2005, 2007). The results of pull tests indicated that in the most cases, except when a high strength concrete or very weak adhesive was used, the cracking in the concrete layer adjacent to the adhesive layer caused the failure of a FRP-to concrete bonded joint. Tests have shown that the de-bonding of FRP from generally occurs within a thin layer of concrete adjacent to the adhesive layer. These results highlight the need for an analytical model that can account for the development of the de-bonding mechanism to accurately simulate the structural response and behavior of walls with the externally bonded FRP reinforcement. Many theoretical models have been developed from 1996 onwards to predict the bond strengths of FRP-concrete bonded joints, generally on the basis of pull test results (Lu *et al.* 2005, 2007).

Lu *et al.* provided a critical review and evaluation of the existing bond strength models and bond-slip models (Lu *et al.* 2005, 2007). The bond-slip models created a new approach in finite element results, with appropriate numerical smoothing, that could be used together with experimental results. This bond-slip behavior of externally bonded FRP strips and concrete was modeled by a relationship on the basis of the fracture energy method. Fig. 3 shows the bond-slip relationships for FRP concrete interfaces (Cruz-Noguez *et al.* 2014, Lu *et al.* 2005, 2007).

The simplified model was made to describe the bond-slip behavior. For this purpose, a bilinear bond-slip curve was used to achieve a simple equation for the bond strength. This bilinear model had the total interfacial fracture energy and the same local bond strength, so this simplification has no effect on bond strength when the bond length was longer than the effective bond length. This bilinear model is shown in equations (Lu *et al.* 2005)

$$\tau = \tau_{max} \left(\frac{s}{s_0} \right) \quad \text{if } s \leq s_0 \quad (3)$$

$$\tau = \tau_{max} \left(\frac{s_f - s}{s_f - s_0} \right) \quad \text{if } s > s_0$$

Where

$$\tau_{max} = 1.5\beta_w f_t \quad (4a)$$

$$s_0 = 0.0195\beta_w f_t \quad (4b)$$

$$G_f = 0.308\beta_w^2 \sqrt{f_t} \quad (4c)$$

$$s_f = \frac{2G_f}{\tau_{max}} \quad (4d)$$

$$\beta_f = \sqrt{\frac{(2.25 - \frac{b_p}{b_c})}{(1.25 + \frac{b_p}{b_c})}} \quad (4e)$$

$$f_t = 0.7\sqrt{f'_c} \quad (5)$$

Where: τ =shear bond stress (MPa), s =interfacial slip (mm), b_f =width of the strip of FRP laminate (mm), b_c =width of the concrete member (mm) in which the FRP strip is located, f_t =tensile strength of concrete (MPa), and G_f =interfacial fracture energy (MPa).

It is important to say that this finite element modelling approach relies on the exact modelling of concrete failure near the adhesive layer.

In this study, for modeling the FRP de-bonding, the cohesive element was used. ABAQUS offers cohesive elements to model the behavior of situations in which the integrity and strength of interfaces may be of interest, like adhesive joints and interfaces in the composite. Cohesive elements are useable in modeling adhesives and bonded interfaces. The response of these elements depends on the special usage and is based on certain assumptions about the deformation and stress states that are proper for each usage

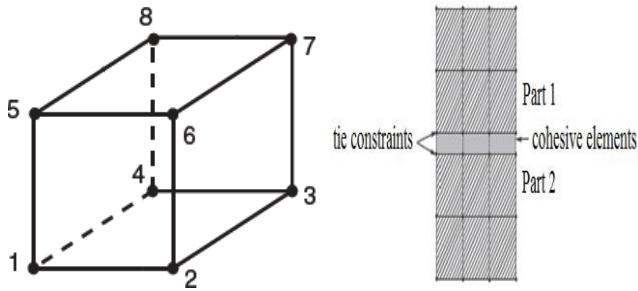


Fig. 4 Details of cohesive element (adapted from ABAQUS 2012)

area. The mechanical constitutive response may be classified based on a traction-separation description of the interface. The cohesive elements model the initial loading, the initiation of damage, and the propagation of the damage leading to the eventual failure at the bonded interface. The behavior of the interface prior to the initiation of damage is often explained as linear elastic in terms of a penalty stiffness that is reduced under tensile and/or shear loading, but is not affected by pure pressure (ABAQUS 2012). The bond-slip curves given by Eqs. (3) and (4) were used to model the shear behavior of cohesive element. concrete tensile behavior (Eq. (5) was used to model the tensile behavior of cohesive elements, and Combination of shear and tensile behavior of cohesive elements model debonding of FRP-strengthened concrete structures. When traction-separation approach is used to model the response of the cohesive elements, the constitutive thickness is assumed to be equal to one by software. This default value shows that the geometric thickness of cohesive elements is often equal to (or very close to) zero for the kinds of applications in which a traction-separation-based constitutive response is appropriate (ABAQUS 2012). The cohesive element was modeled using 8-node 3-D solid elements which had three degrees of translational freedom in each node and meshes of cohesive element was same as meshes of FRP strip. The cohesive element was located between the concrete element and the FRP element. The top and the bottom face of the cohesive element be constrained to another component and the cohesive elements tied to neighboring components (Fig. 4).

2.5 Modeling of damaged element

Damage is usually specified by the degradation of stiffness. An isotropic scaled damage model from the continuum damage mechanics is introduced in ABAQUS to describe the stiffness degradation, which can be represented by Eq. (6) under uniaxial loading (ABAQUS 2012, Tao 2015)

$$\sigma = (1 - d)E_0(\varepsilon - \varepsilon^{pl}) \quad (6)$$

Where: σ , ε , and ε^{pl} represent, respectively, the stress, total strain and plastic strain; E_0 is the initial (undamaged) elastic stiffness; and d is the damage factor, which characterizes the degradation of the elastic stiffness and has values in a range between 0 (undamaged) and 1 (fully damaged). The current degraded stiffness E is defined as

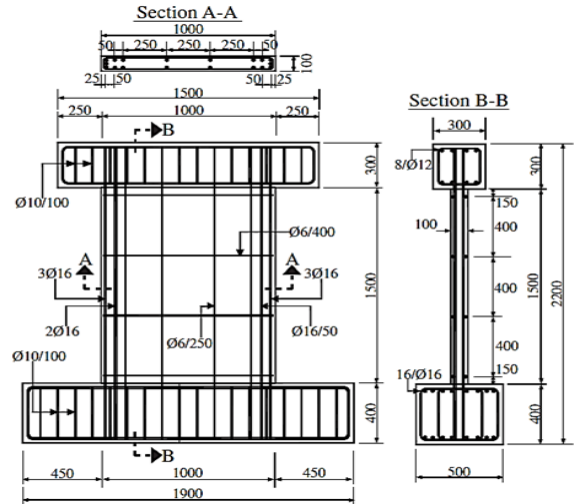


Fig. 5 Reinforcement details of shear walls S1 and S2 (adapted from Altin *et al.* 2013); dimensions in millimeters

(ABAQUS 2012, Tao 2015)

$$E = (1 - d)E_0 \quad (7)$$

This stiffness degradation in concrete element and cohesive element shows concrete damage and FRP debonding respectively.

3. Verification study

In order to confirm the applicability of the proposed finite element model used in this study, it was calibrated and verified with the experimental data. There were a number of experimental tests available in the literature which could be used for the primary verification of the numerical model. For this reason, two shear walls and two strengthened shear walls by FRP strips were simulated by numerical concrete damage plasticity model and the results were compared with the experimental ones. The comparisons were represented by lateral load-top displacement curves and figures describing the failure mode of analytical and experimental specimens. The analysis was performed based on displacement control procedure. These verification studies are presented in the following sections. The analysis was performed based on the displacement control procedure. Loading was applied step-by-step and the analysis is terminated when due to numerical instabilities, the solution was accompanied with serious errors and in some cases stop. In fact, end of analysis was taken when the stiffness of some critical elements was seriously reduced and therefore, a part of model was changed to deal with mechanism and experiments instabilities, leading to an abrupt jump or a negative slope in the load-displacement curve.

3.1 Shear walls S1 and S2 (Altin *et al.* 2013)

These walls were experimentally tested by Altin *et al.* (2013). Section and reinforcement details of the walls are

Table 1 Properties of reinforcements (Data from Altin *et al.* 2013)

| Reinforcement diameter (mm) | Yield strength f_{sy} (MPa) | Failure strength f_{su} (MPa) |
|-----------------------------|-------------------------------|---------------------------------|
| 6 | 325 | 420 |
| 10 | 430 | 522 |
| 12 | 428 | 515 |
| 16 | 425 | 520 |

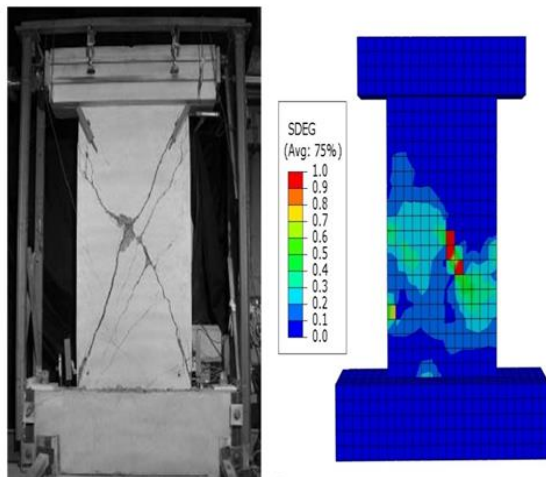


Fig. 6 Comparison of the fracture pattern for shear wall S1 in the experimental study (adapted from Altin *et al.* 2013) and the numerical study

given in Fig. 5. Both walls had identical geometric dimensions and reinforcement layout. Specimens consisted of three structural parts, namely, the head beam through which the lateral loads were transferred into the wall, the panel which modeled a shear wall, and the footing that was used for the anchoring the specimen onto the basement. The concrete cylinder strength was measured to be 15.5 MPa. The reinforcement properties are given in Table 1. The walls were subjected to a lateral load applied through displacement control. Shear wall S1 was the reference specimen tested without strengthening.

The wall was numerically simulated using the previously explained constitutive laws for concrete and reinforcement. The measured maximum lateral force and the corresponding displacement in the reference wall were 149 kN and 7.6 mm, respectively. On the other hand, the numerical predictions obtained for maximum lateral force and the corresponding displacement were 151 kN and 6.08 mm, respectively. The fracture pattern at the ultimate load for the experimental and analytical specimens has been compared in Fig. 6. The variable SDEG (Scalar stiffness degradation), which can take values in the range from zero (undamaged material) to one (fully damaged material) shows the fracture pattern of concrete elements (ABAQUS 2012). It can be observed that the analytical model could simulate the cracking pattern along the height of wall with good accuracy. The experimental and analytical load-displacement responses were compared through the load-displacement curves, as shown in Fig. 7. The results showed that the model was reasonably capable of simulating

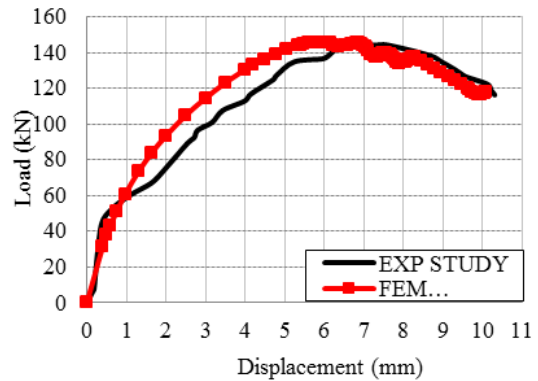


Fig. 7 Comparison of FEM analysis and experimental load-displacement curves of shear wall S1 (adapted from Altin *et al.* 2013)

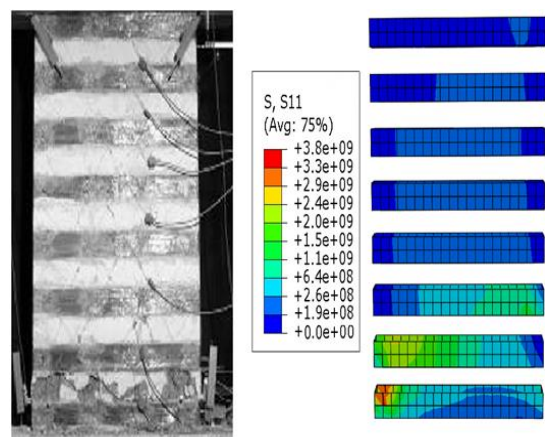


Fig. 8 Shear wall S2 after failure in the experimental study (adapted from Altin *et al.* 2013) and the numerical study (S11 (Pa): stress in fiber direction)

the entire steps of the nonlinear behavior of the concrete shear wall.

The shear wall S2 was tested after strengthening with CFRP strips. The detailed of the applied CFRP configuration are given in Fig. 8. A 200 mm spaced and 100 mm wide lateral wrapped strips were used for the strengthening of shear wall S2. The properties of the CFRP strips included tensile strength (3840 MPa), elastic modulus (231 GPa) and the ultimate strain of the fabric (12.1×10^{-3}), with an average thickness of 0.11 mm and the properties of resin included (30 MPa) and elastic modulus (3800 MPa). It is worth mentioning that in most FRP wrapped, the observed failure mode has been FRP rupture. Therefore, in simulation of this wall, de-bonding of FRP strips was not considered. Concrete was modeled as confined due to the presence of additional stirrups. The finite element analysis resulted in the peak load and the corresponding displacement of 252 kN and 11.76 mm, which was in 2% and 0.2% error of the experimental result of 249 kN and 11.73 mm, respectively. The mechanism of failure at the ultimate load for the experimental and analytical specimens was due to FRP rupture near the base of wall (Fig. 8 shows ultimate stress in fiber direction, as can be seen from this figure stress in FRP strip near the base of wall reached the ultimate stress and fiber ruptured). It was observed that the

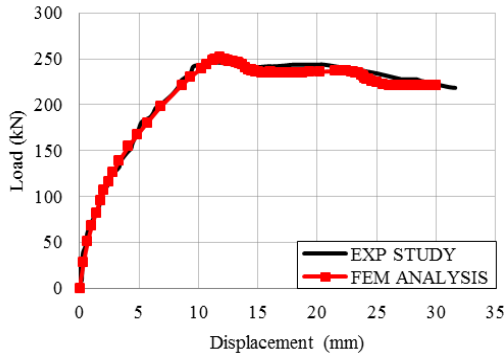


Fig. 9 Comparison of FEM analysis and experimental (adapted from Altin *et al.* 2013) load-displacement curves of shear wall S2

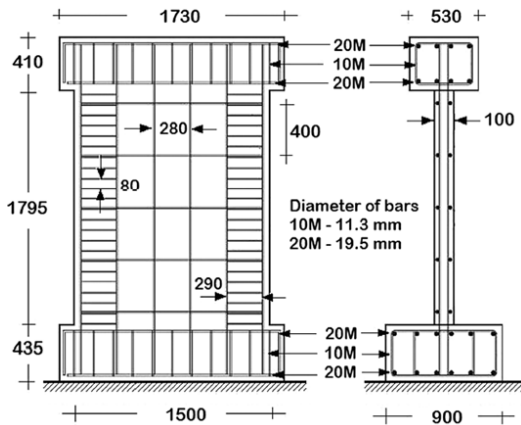


Fig. 10 Reinforcement details of shear walls CW and SW (adapted from Cruz-Noguez *et al.* 2014); dimensions in millimeters

analytical model could simulate the FRP rupture in wrapped FRP strips. The experimental and analytical load-displacement responses were compared through the load-displacement curves, as shown in Fig. 9.

3.2 Shear walls CW and SW (Cruz-Noguez *et al.* 2014)

To evaluate the ability of the numerical model used in this study to model the de-bonding phenomena, CW and SW walls were selected. Shear walls CW and SW were tested by Cruz-Noguez *et al.* (2014). The studied walls were one control wall (CW), and one strengthened wall (SW). The walls were subjected to lateral load applied through displacement control, so a lateral load was applied at the top of the wall using a hydraulic jack and the setup did not include axial load. Cross Section and reinforcement of the walls are shown in Fig. 10. Material properties of concrete, steel, and FRP fibers are given in Table 2.

Base on the literature, confined concrete was used for the concrete at the boundaries of the wall was modeled as confined concrete (Fig. 10), while, the wall core concrete was modeled as unconfined concrete.

The measured maximum lateral force and the corresponding displacement in the control wall were 249 kN and 11.73 mm, respectively. On the other hand, the

Table 2 Material Properties (Data from Cruz-Noguez *et al.* 2014)

| Concrete and steel rebar | | CFRP | |
|--------------------------|---------|------------------------|----------|
| Material property | Value | Material property | Value |
| F'_c | 41 MPa | $f_{FRP,u}$ -Dry fiber | 3.84 GPa |
| F'_y | 412 MPa | E_{FRP} -Dry fiber | 230 GPa |
| ϵ_y | 0.0026 | Et-Epoxy resin | 717 MPa |
| f_u | 654 MPa | f_t - Epoxy resin | 12 MPa |
| ϵ_u | 0.15 | $t_{Laminate}$ | 1.0 mm |

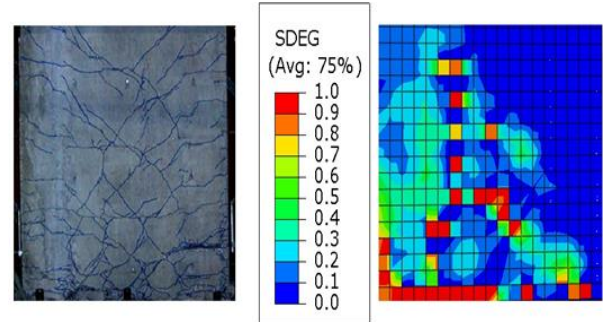


Fig. 11 Comparison of fracture pattern for shear wall CW in the experimental (adapted from Cruz-Noguez *et al.* 2014) and numerical study

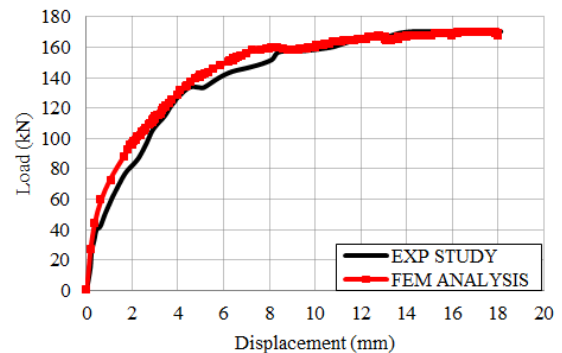


Fig. 12 Comparison of FEM analysis and experimental (adapted from Cruz-Noguez *et al.* 2014) load-displacement curves for the shear wall CW

numerical predictions obtained for the maximum lateral force and the corresponding displacement were 252 kN and 11.76 mm, respectively. Fig. 11 shows the fracture pattern in the experimental and analytical model. The structural response in terms of fracture pattern and load-displacement curve was also predicted by the model, Fig. 12.

Shear wall SW was strengthened by FRP strips oriented in the vertical direction prior to testing. In this wall, the strips were not wrapped around the wall but attached to the front and back faces only. Fig. 13 presents the results obtained using the de-bonding criterion given by Eqs. (3) and (4) in the shear wall SW. This figure shows scalar stiffness degradation (SDEG) of cohesive element which can take values in the range from zero (undamaged material) to one (fully damaged material) shows the failure of cohesive elements. This figure shows a good prediction of the analytical model from failure mechanism. Failure in

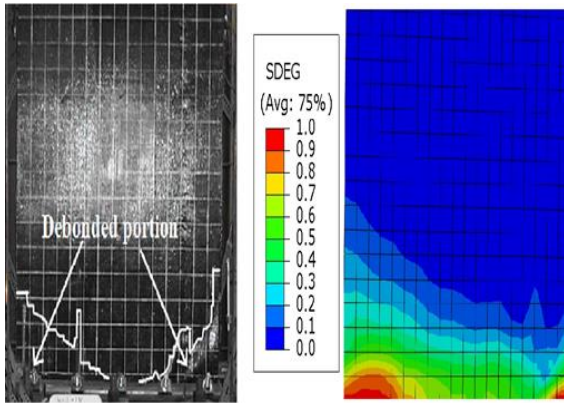


Fig. 13 Comparison of de-bonding portion for the shear wall SW in the experimental study (adapted from Cruz-Noguez *et al.* 2014) and the analytical study

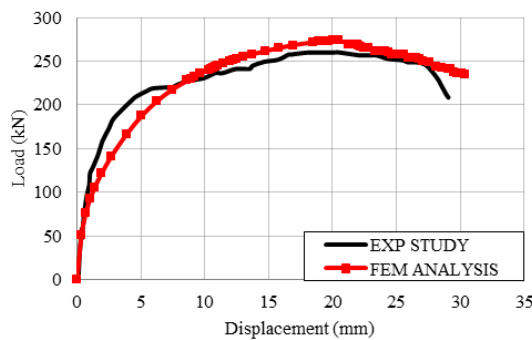


Fig. 14 Comparison of FEM analysis and experimental load-displacement curves for the shear wall SW (adapted from Cruz-Noguez *et al.* 2014)

the experimental study and the analytical model was controlled by de-bonding of the FRP strips at the edges of the wall and there was a satisfactory correspondence between the analytical and experimental results. Fig. 14 shows that the load-displacement responses calculated for shear wall SW agreed closely with the measured results. The differences between the analytical and experimental maximum load and ultimate displacement were 6 and 1%, respectively. It could be seen that the predicted response was in excellent agreement with the experimental behavior. Therefore, the proposed numerical modeling method could be reasonably used for analyzing the FRP strengthened shear walls with opening.

3.3 Mesh-sensitivity study

Element size investigation is an important part for the stability and convergence of the FE results; for this reason, element sizes of 50×50×50, 75×75×75 and 100×100×100 mm were investigated. The results from an analysis on specimen CW, using these three different mesh sizes, are shown in Fig. 15. These element mesh sizes showed acceptable convergence. An element size of 50×50×50 to 100×100×100 mm was used in this paper.

4. Parametric study

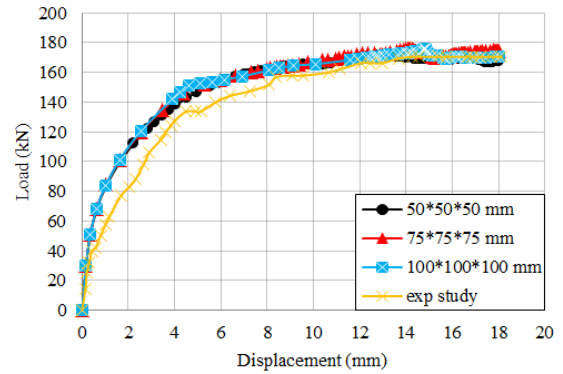


Fig. 15 Mesh sensitivity study

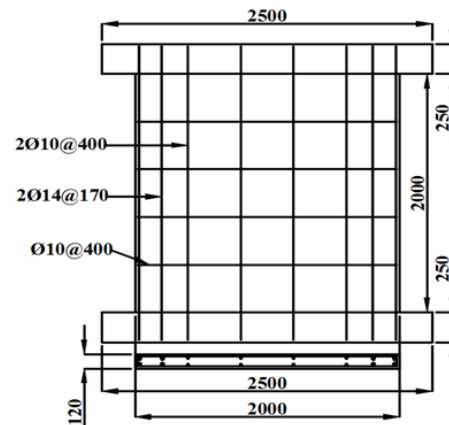


Fig. 16 Reinforcement details of shear wall W1; dimensions in millimeters

Table 3 Comparison of ACI 318 calculated strength and finite element analysis results

| Shear wall | f_c (MPa) | Φ | V_n (kN) | V_u (kN) | M_n (kN.m) | M_u (kN.m) | V (kN) | M (kN.m) | Ratio ^a (%) |
|------------|-------------|--------|------------|------------|--------------|--------------|----------|------------|------------------------|
| W1 | 30 | 0.75 | 333 | 250 | 666 | 500 | 349 | 698 | 95 |

*Note: V_n =Nominal shear strength provided by wall, $V_n=V_c+V_s$, where: V_c is nominal shear strength provided by concrete: $V_c = \frac{1}{4} \sqrt{f_c'} h d + \frac{N_u d}{4 l_w}$, (h =overall thickness or height of member, l_w =length of wall, N_u =factored axial force normal and $d=0.8l_w$), and V_s is nominal shear strength provided by reinforcement: $V_s = \frac{A_v f_y d}{s}$, (A_v =area of shear reinforcement spacing s); Φ =strength reduction factor; V_u =factored shear strength provided by wall, $V_u \leq \Phi V_n$; M_n =nominal moment strength provided by wall; M_u =factored moment strength provided by wall, $M_u \leq \Phi M_n$; V =finite element shear strength provided by wall; M =finite element moment strength provided by wall.

^aRatio of ACI-318 capacity values (V_u) to finite element capacity values (V).

After verification of the proposed model, in order to study the effects of FRP strengthening in shear walls with opening, one squat shear wall with opening was strengthened by CFRP strips with different configurations and thicknesses of strips. In this study, the lateral force transfer mechanisms in the walls were the focus; therefore,

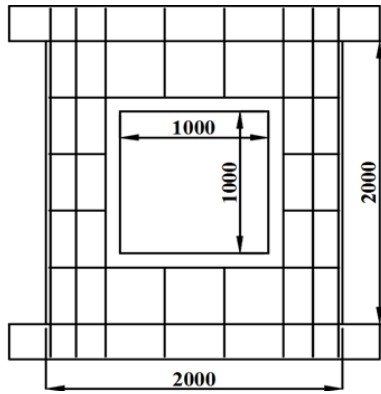


Fig. 17 Reinforcement details of shear walls W1O; dimensions in millimeters

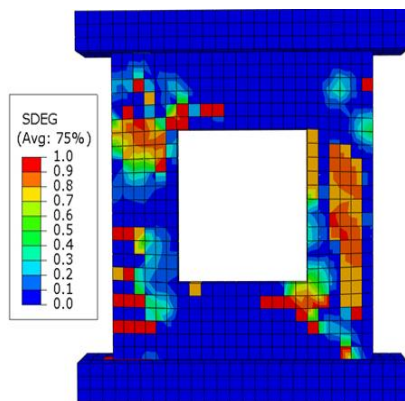


Fig. 18 Failure pattern for the shear wall with opening (W1O)

all studied walls were subjected to lateral load applied through displacement control and no axial force was applied.

4.1 Shear wall W1

This shear wall was designed according to ACI 318-11. Dimensions and reinforcement details of this wall are given in Fig. 16. The wall consisted of three structural parts, namely, the head beam through which the lateral load was transferred into the wall, the panel which modeled a shear wall and the footing which was used for anchoring the specimen onto the basement. The head beam and base beam had the cross-section of 250×400 mm. Wall length, height and thickness were $l=2000$ mm, $h=2000$ mm, and $t=120$ mm, respectively. The aspect ratio of the wall (h/l) was 1, so the wall, based on ASCE 41-06, was a squat wall (ASCE 41 (2006)). The concrete compressive strength was 30 MPa and steel bars with the nominal yield strength of 460 MPa and the ultimate strength of 600 MPa were used.

Comparison of ACI 318 Calculated Strength and finite element analysis results are given in Table 3.

Based on the ACI 318, when the maximum extreme compressive stress, corresponding to factored forces exceeds $0.2 f_c'$ shear wall need to have boundary elements at boundaries (ACI Committee 318 2011). In the shear wall W1 the calculated compressive stress was less than $0.2 f_c'$, so this wall didn't need the boundary elements.

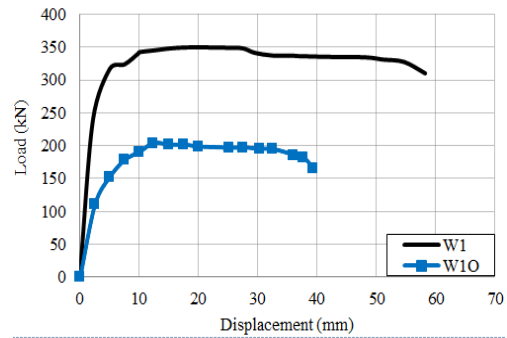


Fig. 19 Comparison of load-displacement curves for the shear walls W1 and W1O

Table 4 Material properties of FRP strips

| CFRP composite | Elastic modulus (GPa) | Poisson's ratio | Tensile strength (MPa) | Thickness of laminate (mm) |
|----------------|-----------------------|-----------------|------------------------|----------------------------|
| | $E_x=231$ | $\nu_{xy}=0.22$ | | |
| CFRP | $E_y=38$ | $\nu_{xz}=0.28$ | 4100 | 1 |
| | $E_z=38$ | $\nu_{yz}=0.28$ | | |

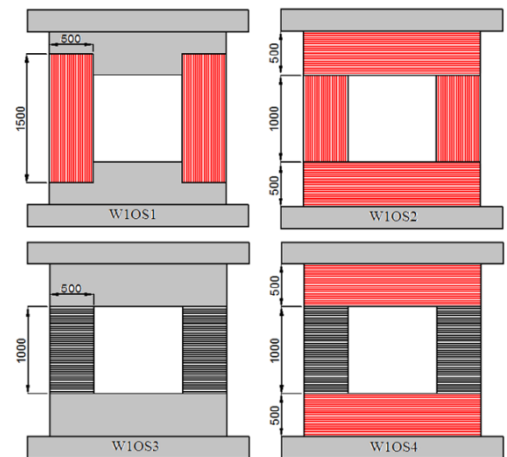


Fig. 20 Strengthening schemes of walls; dimensions in millimeters

4.2 Shear wall W1O

In order to study the effects of opening in the lateral behavior of the squat shear wall, one square opening was considered in the center of the shear wall W. As previously mentioned, opening was not considered during structural design of the wall and the steel reinforcement intercepted by the opening was cut. The shear wall with opening was named W1O. Based on ASCE 31-03 (2003), openings shall constitute less than 75% of the length of any perimeter wall for life safety and 50% immediate occupancy with wall piers having the aspect ratios of less than 2, so in this study, the size of opening was assumed to be 50% of the length of wall. Dimensions of the opening and reinforcement details of this wall are shown in Fig. 17.

The final fracture pattern of Specimen W1O is illustrated in Fig. 18. It can be observed that when opening was created in the shear wall, the concentration of fracture was around the opening, especially in piers, and the failure of wall was occurred at these places; in particular,

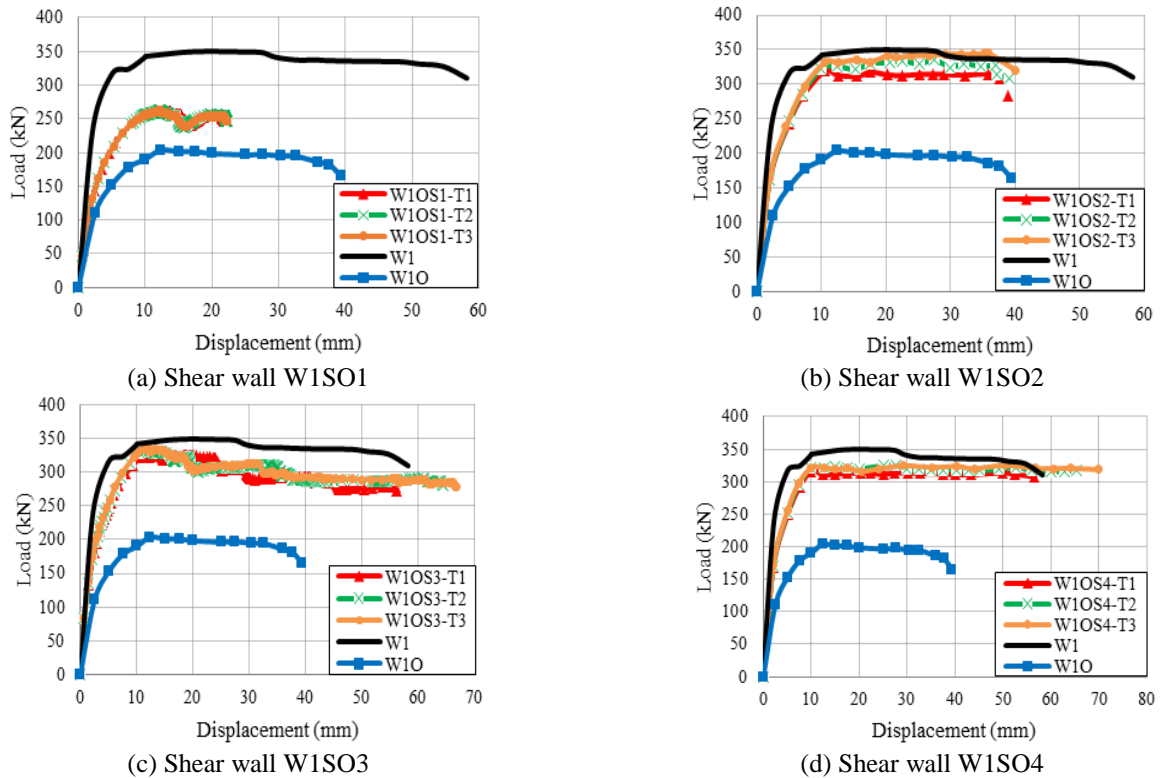


Fig. 21 Load-top displacement curve from the numerical analysis of the strengthened shear walls

extremely severe concrete fracture was observed at two piers near to the opening. Load-lateral displacement curves for the shear walls W1 and W1O are shown in Fig. 19. As can be seen, lateral load carrying and ultimate lateral displacement capacity were significantly decreased in W1O. It can also be observed that when specified opening was inserted in the shear wall, maximum lateral load capacity and the ultimate displacement at the top of the wall were decreased by 41% and 32%, respectively.

4.3 The effect of FRP strengthening of squat shear wall with opening

In order to investigate the efficiency of the strengthening of squat shear walls with opening by FRP strips, 4 FRP strengthened walls were studied (shear walls W1OS1-W1OS4). The specimens were loaded after strengthening with four different configurations of CFRP strips. The detailed descriptions of applied CFRP configurations are given in Fig. 20. To study the effects of flexural strengthening of shear wall with opening, a layer of CFRP strips (1500 mm length) was applied at each pier with fibers oriented in the vertical direction for the strengthening of shear wall W1OS1. CFRP strips were applied around the opening for the shear wall W1OS2, 500 mm wide CFRP strips with fibers oriented in the horizontal direction were applied to the top and bottom of opening for shear strengthening and cover the top and bottom of the shear wall for providing more anchoring and 1500 mm length CFRP strips were applied at each pier with fibers oriented in the vertical direction for flexural strengthening. To study the effects of stirrups in shear wall with opening, a

layer of CFRP strips was wrapped around each pier like stirrups for the shear wall W1OS3. Similar CFRP strips were used for the shear wall W1OS4 and 500 mm wide CFRP strips with fibers oriented in the horizontal direction were applied to the top and bottom of the opening to cover the top and bottom of the shear wall for providing more anchoring and preventing fracture at the corner of the opening. In the shear walls W1OS1, W1OS2 and W1OS4, strips were applied on both faces of the walls. To investigate the effect of the thickness of FRP strips in strengthening of shear wall with opening, 3 different thicknesses was used. The thickness of CFRP used to strengthen the shear walls was T1, T2 and T3, equal to 1, 2 and 3 mm, respectively. Names of the models were based on the location of the CFRP strips and the thickness, respectively. Table 4 illustrates the mechanical properties of the CFRP.

4.4 Results of finite element analysis of the strengthened walls

Load-displacement curves for the shear walls specimens are shown in Fig. 21. These figures indicate that lateral displacement, lateral load carrying and energy dissipation capacities were significantly increased. For the strengthened shear wall W1OS1, figure shows the strengthening of the wall improved the wall lateral load capacity (about 28%), whereas the lateral resisting capacity of the strengthened wall was higher than that of W1O but the ultimate displacement of the wall decreased because of the premature de-bonding of CFRP strips. As can be seen in this figure, increasing the CFRP thickness did not have

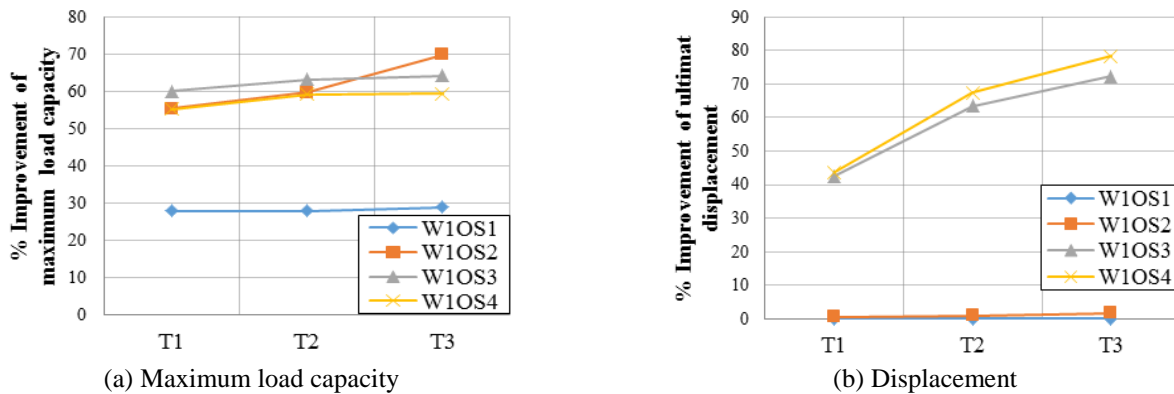


Fig. 22 Improvement of the maximum load capacity and ultimate displacement of all wall specimens

Table 5 A summary of studied CFRP strengthening schemes

| Specimen | Ultimate Displacement (mm) | Maximum load carrying capacity (kN) | Ultimate Displacement improvement (%) | Maximum load carrying capacity improvement (%) | Ultimate failure mode |
|----------|----------------------------|-------------------------------------|---------------------------------------|--|--------------------------|
| W1OS1-T1 | 21 | 261 | 0 | 28 | FRP de-bonding |
| W1OS1-T2 | 21 | 261 | 0 | 28 | FRP de-bonding |
| W1OS1-T3 | 22 | 262 | 0 | 29 | FRP de-bonding |
| W1OS2-T1 | 39 | 316 | 0 | 55 | FRP de-bonding |
| W1OS2-T2 | 39 | 325 | 1 | 59 | FRP de-bonding |
| W1OS2-T3 | 40 | 245 | 2 | 69 | FRP de-bonding |
| W1OS3-T1 | 56 | 326 | 42 | 60 | FRP rupture |
| W1OS3-T2 | 64 | 332 | 63 | 63 | FRP rupture |
| W1OS3-T3 | 67 | 334 | 72 | 64 | FRP rupture |
| W1OS4-T1 | 56 | 316 | 43 | 55 | FRP rupture & de-bonding |
| W1OS4-T2 | 65 | 325 | 67 | 59 | FRP rupture & de-bonding |
| W1OS4-T3 | 70 | 325 | 78 | 59 | FRP rupture & de-bonding |

considerable effect on the overall behavior of the wall since failure of the strengthened shear wall was due to FRP de-bonding which was concentrated in the edge of piers. It can be observed in the figure that the lateral resisting capacity of W1OS2 was significantly higher than that of the corresponding control shear wall W1O (about 59%). CFRP strips controlled the fracture and the maximum lateral load of the strengthened wall was almost equal to that of the shear wall with no opening (W1) and shear wall was reached its flexural capacity. Horizontal FRP strips were prevented the premature de-bonding of CFRP strips from the wall surfaces and lateral deformation was improved than shear wall W1OS1. As can be seen in the figure, increasing the thickness of CFRP strips led to slightly increase in maximum applied load and did not show significant effect on the ultimate displacement of the wall. Shear wall W1OS2 failed due to the separation of CFRP strips from the wall surface and the de-bonding was concentrated around the top and bottom of opening. The load displacement curves of the shear wall W1OS3 are shown that the lateral resisting capacity of W1OS3 was larger than that of corresponding control wall W1O. The lateral load capacity

and ultimate displacement compared to W1O increased by 60 and 42%, respectively. In this configuration, CFRP strips were wrapped around the piers and effectively confined the concrete. It is observed that when CFRP strips wrapped around the piers, the concrete behavior was improved and due to this configuration, the ultimate lateral load capacity of the wall was increased to as high as that of wall with no opening, W1. Failure of W1OS3 was due to FRP rupture in piers edge. The shear wall W1OS4 is shown the improvement of lateral load carrying capacity and lateral displacements were significantly increased (55% and 43%, respectively). Lateral load capacity and the ductility for the strengthened wall were almost equal to that of shear wall without opening. CFRP strips which were wrapped around the piers confined the concrete and horizontal CFRP strips improved the inelastic behavior in the load displacement curve. In this wall, increasing the thickness of CFRP mostly lead to increase of the ultimate lateral displacement. Failure of this wall was due to rapture of FRP strips in edge of piers and FRP de-bonding at the top and bottom of the opening.

Table 5 compares the computed and measured results of the maximum load and the ultimate displacement for each of the studied strengthening schemes.

Fig. 22(a) and (b), show the improvement of maximum lateral load capacity and ultimate lateral displacement, respectively. As can be seen from these figures, shear walls W1OS3 and W1OS4 showed the most suitable performance in load capacity and ductility among all studied strengthened walls.

5. Conclusions

There are situations in which an opening needed to be provided in a constructed shear wall. Since the opening has not been considered in structural design of the wall, therefore it is necessary to study the effect of opening on lateral load carrying capacity and lateral displacement capacity of the wall. In most cases strengthening of the wall would be necessary.

This paper demonstrated the results of nonlinear finite element analysis of CFRP strengthened shear wall with opening. To do this study a numerical model was developed and verified. Six shear wall specimens were studied, two of them were the shear wall without CFRP strengthening, and rest of them were strengthened by using four different

CFRP strip configurations. All shear walls were tested under monotonic lateral loading. In this study, the prediction capacity of the bond slip model was verified. From this study, the following results can be concluded:

- Concrete damage plasticity model could predict the lateral load-displacement of a shear wall in all linear and nonlinear stages of its behavior accurately.

- Creating openings with the size of 50% of the length and height of the wall, in a constructed wall without considering its effect in the structural design of the wall, resulted in a load capacity and ultimate displacement reduction of about 42.1% and 32%, respectively.

- The proposed methods for the FE modeling of the FRP strips and the bond interface between the FRP and concrete provided a good correlation to experimentally observed responses and numerical bond slip modeling method was successfully implemented to predict the de-bonding mechanisms.

- Based on the results, applying vertical FRP strips on piers of the wall was effective in significantly increasing the lateral load carrying capacity of the wall. On the other side, wrapping CFRP strips around the piers resulted in significant improvement in both lateral load carrying capacity and ultimate lateral displacement and ductility of the wall.

- FRP-concrete de-bonding mechanisms were important factors that significantly influence the capacity of the strengthened walls.

- The strip configurations highly affected the behavior and failure mode of the strengthened wall. The most improvement in lateral displacement capacity and lateral strength of the shear wall with opening was obtained by CFRP wrapping of piers.

- Increasing the thickness of CFRP strips was mostly effective on the ultimate lateral displacement of walls strengthened by wrapped CFRP strips.

References

- ABAQUS 6.12 (2012), *ABAQUS User's Manual*, Providence, Rhode Island, U.S.A.
- ACI 318 (2011), *Building Code Requirements for Structural Concrete and Commentary*, Farmington Hills, Michigan, U.S.A.
- ACI 440.2R (2008), *Guide for the Design and Construction of Externally Bonded FRP Systems for Strengthening Concrete Structures*, Farmington Hills, Michigan, U.S.A.
- Altin, S., Anil, Ö., Koprman, Y. and Kara, M.E. (2013), "Hysteretic behavior of RC shear walls strengthened with CFRP strips", *Compos. Part B: Eng.*, **44**(1), 321-329.
- ASCE 31 (2003), *Seismic Evaluation of Existing Buildings*, America Society of Civil Engineers (ASCE), Reston, Virginia, U.S.A.
- ASCE 41 (2006), *Seismic Rehabilitation of Existing Buildings*, America Society of Civil Engineers (ASCE), Reston, Virginia, U.S.A.
- Behfarnia, K. and Sayah, A. (2012), "FRP strengthening of shear walls with openings", *Asian J. Civil Eng.*, **13**(5), 691-704.
- Chen, W.F. (2007), *Plasticity in Reinforced Concrete*, J. Ross Publication, New York, U.S.A.
- Cruz-Noguez, C., Lau, D. and Sherwood, E. (2014), "Seismic behavior of RC shear walls with externally bonded FRP sheets:

- Analytical studies", *J. Compos. Constr.*, **18**(5), 04014011.
- Cruz-Noguez, C., Lau, D., Sherwood, E., Hiotakis, S., Lombard, J. and Foo, S. (2014), "Seismic behavior of RC shear walls strengthened for in-plane bending using externally bonded FRP sheets", *J. Compos. Constr.*, **19**(1), 04014023.
- Kim, S. and Vecchio, F. (2008), "Modeling of shear-critical reinforced concrete structures repaired with fiber-reinforced polymer composites", *J. Struct. Eng.*, **134**(8), 1288-1299.
- Li, B. and Lim, C. (2010), "Tests on seismically damaged reinforced concrete structural walls repaired using fiber-reinforced polymers", *J. Compos. Constr.*, **14**(5), 597-608.
- Li, B., Qian, K. and Tran, C. (2013), "Retrofitting earthquake-damaged RC structural walls with openings by externally bonded FRP strips and sheets", *J. Compos. Constr.*, **17**(2), 259-270.
- Li, Z.J., Balendra, T., Tan, K.H. and Kong, K.H. (2005), "Finite element modeling of cyclic behavior of shear wall structure retrofitted using GFRP", *Proceedings of the Fiber-Reinforced Polymer Reinforcement for Concrete Structures*, Michigan, U.S.A., January.
- Lombard, J. (1999), "Seismic strengthening and repair of reinforced concrete shear walls using externally-bonded carbon fibre tow sheets", M.S. Dissertation, Carleton University, Ottawa, Canada.
- Lu, X., Teng, J., Ye, L. and Jiang, J. (2007), "Intermediate crack debonding in FRP-strengthened RC beams: FE analysis and strength model", *J. Compos. Constr.*, **11**(2), 161-174.
- Lu, X.Z., Teng, J.G., Ye, L.P. and Jiang, J.J. (2005), "Bond-slip models for FRP sheets/plates bonded to concrete", *Eng. Struct.*, **27**(6), 920-937.
- Meftah, S.A., Yeghneem, R., Tounsi, A. and Adda, E.A. (2007), "Seismic behavior of RC coupled shear walls repaired with CFRP laminates having variable fibers spacing", *Constr. Build. Mater.*, **21**(8), 1661-1671.
- Mostofinejad, D. and Mohammadi, A.M. (2012), "Effect of confining of boundary elements of slender RC shear wall by FRP composites and stirrups", *Eng. Struct.*, **41**, 1-13.
- Reddiar, M.K.M. (2009), "Stress-strain model of unconfined and confined concrete and stress-block parameters", M.S. Dissertation, Texas A&M University, Texas, U.S.A.
- Rezaiefar, A. (2013), "Finite element modeling of cyclically loaded FRP retrofitted RC squat shear walls", M.S. Dissertation, Concordia University, Montreal, Canada.
- Sengupta, P. and Li, B. (2014), "Hysteresis behavior of reinforced concrete walls", *J. Struct. Eng.*, **140**(7), 04014030.
- Shariq, M., Abbas, H., Irtaza, H. and Qamaruddin, M. (2008), "Influence of openings on seismic performance of masonry building walls", *Build. Environ.*, **43**(7), 1232-1340.
- Tao, Y. and Chen, J. (2015), "Concrete damage plasticity model for modeling FRP-to-concrete bond behavior", *J. Compos. Constr.*, **19**(1), 04014026.

SF